(2)

Fairfax Materials Research Inc.

5613 Marble Arch Way
Alexandria, Virginia 22310-4011

(703)-922-4579 Fax: (703)-922-6034

November 16 1992

Dr. A. K. Vasudevan, code 1222
Office of Naval Research
800 N. Quincy Street
Arlington, VA 22217-5000

re: Contract #N00014-91-C-0067

Dear Dr. Vasudevan:

Please find attached one copy of the November 16 report on the above contract, as specified in your letter of August 7 (your ref: 3900 Ser 1222/01) and in accordance with the contract above.

Yours sincerely

Dr. M.S. Duesbery
Vice-President
Fairfax Materials Research, Inc.

cc: ACO
NRL
DTIC (2)
CTM

Computer Modelling of Cyclic Deformation of High-Temperature Materials
TECHNICAL PROGRESS REPORT

Dr. M.S. Duesbery
Principal Investigator

Dr. N.P. Louat
Senior Scientist

Fairfax Materials Research, Inc.
5613 Marble Arch Way
Alexandria, VA 22310-4011

November 16, 1992

Period of performance
March 16, 1991 through November 15, 1992

I. Introduction and Program Objective

Current methods of lifetime assessment leave much to be desired. Typically, the expected life of a full-scale component exposed to a complex environment is based upon empirical interpretations of measurements performed on microscopic samples in controlled laboratory conditions. Extrapolation to the service component is accomplished by scaling laws which, if used at all, are empirical; little or no attention is paid to synergistic interactions between the different components of the real environment. With the increasingly hostile conditions which must be faced in modern aerospace applications, improvement in lifetime estimation is mandated by both cost and safety considerations.

This program aims at improving current methods of lifetime assessment by building in the characteristics of the micro-mechanisms known to be responsible for damage and failure. The broad approach entails the integration and, where necessary, augmentation of the micro-scale research results currently available in the literature into a macro-scale model with predictive capability.

In more detail, the program will develop a set of hierarchically structured models at different length scales, from atomic to macroscopic, at each level taking as parametric input the results of the model at the next smaller scale. In this way the known microscopic properties can be transported by systematic procedures to the unknown macro-scale region. It may not be possible to eliminate *empiricism* completely, because some of the quantities involved cannot yet be estimated to the required degree of precision. In this case the aim will be at least to eliminate functional empiricism. Restriction of empiricism to the choice of parameters to be input to known functional forms permits some confidence in extrapolation procedures and has the advantage that the models can readily be updated as better estimates of the parameters become available.

II. Program Organization

The program has been organized into specific tasks and subtasks as follows.

Task 100. Lifetimes of metallic dispersed-phase composites

Most service materials fall into the category of dispersion-hardened metallic composites. This task will consider the problem of dispersion hardened materials in general, but with two specific materials, NiAl and $MoSi_2$/SiC in mind.

Task 110. Identification and modelling of micromechanisms

The purpose of this task is to determine what micromechanisms are operative in the high-temperature deformation of dispersion-hardened materials. In the general case this will be done by a literature search. For specific materials, the micromechanisms will be determined from the experimental program at NRL. Once identified, each of these micromechanisms will be

modelled, in order to determine what are the critical parameters which determine its effect on plastic flow and values for these parameters. Also to be determined is whether the modelled critical values are dependent on quantities which must be obtained from a smaller scale model.

Task 111. Equiaxed dispersoids

This task will consider dispersions of the type encountered in NiAl-like materials. That is, the dispersoids are considered to be small compared to the grain size. The term 'equiaxed' is used because the particles are roughly of the same size in all three dimensions. However, this is not a requirement for this task. Rather, it is necessary that the particles not be too large in the dimension normal to the slip plane, so that they can be surmounted with relative ease by cross-slip and/or climb without the generation of appreciable back-stress.

Task 112. Anisotropic dispersoids

This task covers the case of dispersoids which are elongated in the direction normal to the slip plane. An example is SiC fibers in $MoSi_2$. In this case, plastic flow around the dispersoids takes place by a combination of glide and climb, but is a protracted process during which large stresses acting in opposition to the applied load are developed.

Task 113. Grain boundary effects

This task will examine the role of grain boundary processes in high-temperature deformation.

Task 120. Macroscopic stochastic model for creep

In real materials it is likely that more than one mechanism will be operative, either in parallel or in series. The information gained in task 110 is not sufficient to describe this situation. Once the critical parameters for individual mechanisms have been determined, it is necessary to combine them in a macroscale stochastic model. This will be done by determining critical stresses and activation enthalpies as a function of local geometry and using these values in a finite-temperature simulation of creep through a random array of dispersoids. Careful attention must be paid to possible interactions between mechanisms.

Task 130. Extension to cyclic deformation

The final step in task 100 is to extend the results to the case of cyclic deformation. Irreversibility is an intrinsic feature of the model in task 120. However, it is likely that other, as yet unrecognized, characteristics of cycled deformation will have to be considered.

Task 200. Lifetimes of piezoelectric ferroelectrics

Failure in cyclic loading of sensors and actuators formed from lead zirconate titanate (PZT) is a continuing problem. PZT is a ceramic and therefore differs from the materials considered in

task 100 in that plastic deformation is not involved. This task will examine, modelling as necessary, the operation of PZT devices, in order to determine the factors governing lifetime limitation.

Task 300. Reporting

Running concurrently with tasks 100 and 200, this task will inform the Navy Program Manager and Contracting Officer of the technical and fiscal status of the program through R&D status reports.

III. Technical Progress

Task 111. Equiaxed dispersoids

a. Theory

Hardening of metals by means of second-phase or extrinsic particles, commonly known as dispersion hardening, has been a standard route to improvement of the mechanical properties of metals for many years. There are several distinct mechanisms for the hardening, all of which involve retardation of plastic flow.

- Orowan looping, or the impedance to flow offered by impenetrable obstacles.
- Stacking fault hardening, in which the stacking fault energy inside the obstacle is different from that in the matrix.
- Order hardening, for which the crystal structure within the obstacle forms an ordered superlattice, so that the low-energy deformation route requires paired dislocations.
- Chemical hardening, which results from the surface energy generated when a precipitate is intersected.
- Modulus hardening, due to a mismatch of elastic constants between dispersoid and matrix.
- Coherence hardening, caused by the back-stress from inclusions which do not fit into the holes in the matrix without elastic deformation.

For each of the mechanisms listed above, there exists an approximate theory, usually supportable with a single set of experimental measurements. The experiments themselves are difficult, because the mechanisms are not separable and the range of variables which can be accessed is severely limited. This is not at all a satisfactory foundation on which to build a global deformation model.

Our unified approach, based on extensive computer modelling of individual mechanisms, has been to recognize that the problem is essentially geometric, the primary factors being the size D and spacing L of the dispersoids, as illustrated in Figure 1. The detailed nature of the particular mechanisms is of no practical consequence, and can be accommodated by assigning an intrinsic strength, or impedance, to each obstacle. This intrinsic impedance can also be expressed in geometric terms by the breaking angle θ (see Figure 1). The strength of any dispersed-phase composite then depends only upon the statistical distributions of these three geometric parameters.

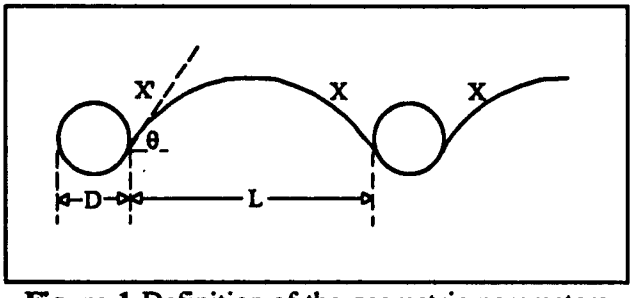

Figure 1 Definition of the geometric parameters D, L and θ.

Work to date has concentrated on regular dispersions, that is, those for which the three parameters L, D and θ are single-valued throughout the material. Even this limited theoretical model gives a better description of the available experimental work than any earlier treatment. Specifically, we have reprocessed or performed computations of the strength of regular arrays for the cases of coherence hardening[1], modulus hardening[2], stacking fault hardening[3] and order hardening[3], in both particle intersection and Orowan looping limits. We find that in all cases the strength is described well by the expression

$$\sigma = \frac{\mu b}{2\pi AL} \ln X \sin\theta \qquad (1)$$

where X is the harmonic mean of D and L, that is

$$\frac{1}{X} = \frac{1}{D} + \frac{1}{L} \qquad (2)$$

and A is a constant which is unity for screw dislocations and $(1-\nu)$ for edge dislocations. Use of the harmonic mean for X, which is the characteristic length describing the elastic energy of the dislocation configuration, reflects the dominant influence on the line energy of the dispersoid and interdispersoid dipoles (formed by the arms XX and X'X, respectively, in Figure 1).

It is important to note that we find equation (1) to be valid for all applied stresses, even those less than the critical values. This means that (1) applies to the creep (unidirectional and cyclic) conditions important to lifetime studies.

b. Comparison with Experiment

There is no question but that the fundamental hardening stems from an Orowan-like impedance and therefore depends, to first order, inversely on the dispersoid separation L. The classical Orowan model, based on elementary line tension theory, predicts the dependence

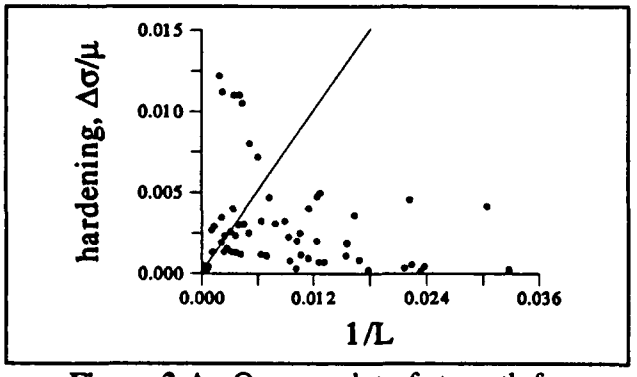

Figure 2 An Orowan plot of strength for dispersion hardened materials.

$$\sigma = \frac{\mu b}{L} \sin\theta \qquad (3)$$

with the breaking angle factor $\sin\theta = 1$. However, a simple plot of the hardening $\Delta\sigma$ against 1/L (Figure 2) reveals that this approximation is grossly inadequate. The experimental data shown in Figure 2 consist of 79 measurements from eight distinct sources[4-11], encompassing all of the hardening mechanisms detailed above. The solid line indicates the theoretical

dependence (3). In principle, a knowledge of the true breaking angles might improve the agreement, but none of the experimental work includes this information, which would require *in-situ* TEM measurements. Suitable values for θ could bring all values below the line in Figure 2 into agreement with (3), but not the many points which lie above the line.

To compare the data with our unified approach, equations (2) and (3), we use the correction for coherent precipitates introduced by Duesbery and Sadananda[1], which defines the effective diameter D* of a coherent obstacle by the relation

$$(\frac{D*}{D})^4 = 0.25L\epsilon \qquad (4)$$

where ϵ is the misfit factor. There remains the problem of the unknown breaking angle. The approach we have taken for this is to use the experimental data to derive the distribution $N(\theta)$ required for the experimental points to fit the theoretical prediction. The results for the data plot are shown in Figure 3. Although the fitting of the breaking angle guarantees that most of the data points will fall exactly on the theoretical line, this is not entirely a trivial exercise. In Figure 3 only two points lie above the theoretical line, and these only just so. This contrasts favorably with the case shown in Figure 2.

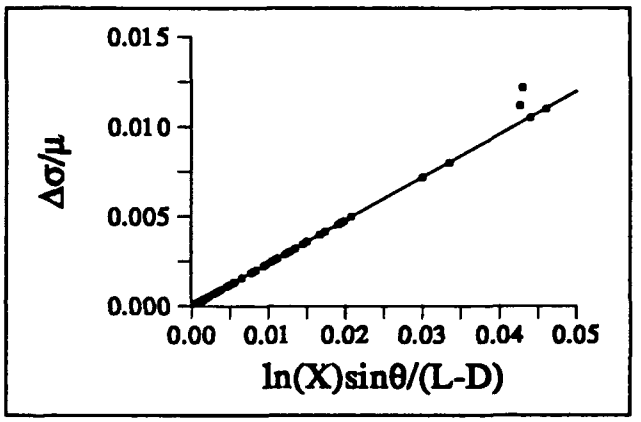

Figure 3 Plot of strength following the unified approach of equation (2).

The distribution $N(\theta)$ is shown in Figure 4. It can be seen that the required breaking angles fall mostly in the range of 10° - 50°, much smaller than the 90° usually assumed, but consistent with the angles observed in computer modelling of coherent[2] and/or penetrable[2,3] dispersoids.

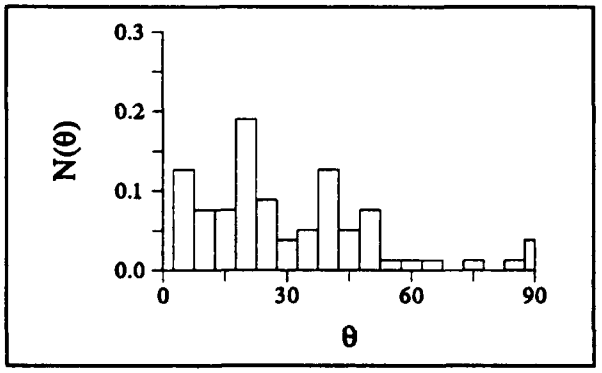

Figure 4 The distribution of breaking angles.

We cannot state unequivocally that the experimental results prove that our unified approach is valid. This is simply because the experimental measurements do not contain enough information for this purpose. However, we can state with confidence that all of the experimental work is consistent with the unified approach.

c. Implications

★ The importance of the unified description (2) is that it applies to all passing mechanisms (with the possible exception of cross-slip and climb), for all dispersed phase composites in which classical dispersion hardening dominates. The utility of the approach is that it permits the ready construction of a global geometric model in which the dispersion is characterized by the characteristic length X and the details of the dislocation-particle interactions are subsumed into the breaking angle distribution $N(\theta)$. This permits the ready calculation of activation enthalpies for plastic flow.

★ The unified description applies not only to ultimate strength estimation, but also to deformation by unidirectional and cyclic creep.

d. Plans

★ Develop this unified approach into a stochastic, high-temperature creep model in two steps:

1. Creep models for specific mechanisms (as defined by the breaking angle) with both regular and random arrays of dispersoids, in order to determine stress exponents for comparison with and analysis of experiments.

2. A combined model for creep through a random array of dispersoids with a spectrum of strengths.

★ Hence compute lifetimes in unidirectional and/or cyclic deformation as estimates of the time required to reach a critical level of damage.

Task 112. Anisotropic dispersoids

An analytic model of the hardening due to elongated fibers, or whiskers, has been developed.

a. Theory

We assume slender cylindrical whiskers of length 2l and radius r to lie parallel to the axis of deformation and not to take part in that deformation. The first assumption does not impact the conclusions significantly. We further suppose that the material in which the whiskers are imbedded, strains uniformly at a rate ϵ. This deformation is achieved by processes which differ in detail with distance from the interface of the non-deforming cylinders. At remote positions deformation is achieved simply by dislocation glide. In the neighborhood of a cylinder and specifically at distances from the surface of the order of interatomic spacings, glide is inhibited and is replaced by 'glimb' (a combination of glide and climb, possibly alternating) while individual dislocations form elliptical loops which circumnavigate the perimeter of a particular cylinder. Each such loop retains its own characteristic Burgers vector, but the mean direction of all such Burgers vectors is parallel to the direction of straining. Then referring our considerations to the steady state in which incremental strain is everywhere continuous we require that the net forces and motion of the glimbing dislocations be parallel to the interface and that the number of dislocation of magnitude b which glimb past a point distant x from the mid point of a whisker be

$$\frac{\dot{x}}{b} = f(x)v(x) \tag{5}$$

where v(x) is the dislocation velocity and f(x) the density (that is the number of dislocations of magnitude b per unit length) at the said position x. The force acting per unit length (L) of any dislocation is

$$F = \sigma b L \tag{6}$$

when the stress σ and the Burgers vector, of magnitude b, are so disposed that the force on the dislocation is in the direction of the Burgers vector. Here, as stated above, the mean direction of the Burgers vectors of all dislocation loops is parallel to the axis of strain and we shall in the first instance suppose that this direction is parallel to that of the axes of the cylinders. Taking advantage of the fact that this model requires that these dislocations move parallel to this same direction we replace, fo the purposes of calculation of stresses, the actual arrangement of elliptical dislocation loops with a continuum of circular loops, having displacement vectors parallel to the mean of their directions and this to the axes of the cylinders. We further require that the glimb of these dislocations involve the emission and absorption of vacancies and thus the processes of diffusion. To the extent that the velocity resultant on the application of a force may be regarded as the consequence of an Einstein drift it is given by

$$v = \frac{DF}{kT} = \frac{Db\sigma}{kT} \tag{7}$$

where D is the coefficient of self diffusion of the matrix, k is Boltzmann's constant and T the temperature. Since the dislocation motion is restricted by the need for climb it can be. argued that F should be identified as the force available for that motion. However, it would seem likely that the actual motion would be clearly separable into climb and glide over only very short lengths (i.e. a few Burgers vector distances) with the result that the force available would be that for the mean motion. The stresses developed on the glimbing dislocations are given by

$$\sigma(x) = -\frac{\mu b}{2\pi(1-\nu)}\int_{-l}^{l} f(t)G(t,x)dt \tag{8}$$

Because the dislocations which surround the cylinder are taken to be circular loops, with Burgers vectors normal to the planes of the loops we see that the stress relevant in the calculation of the force parallel to the axis of the cylinders is that for shear. The stress from such a loop has been calculated by Kroupa[12]. However, one may as first approximation avoid the usage of the complicated representation of the stresses by recognizing that for small values of t-x, that is when the factor h = (t -x) /r $<<$ 1, that

$$G(t,x) = \frac{1}{t-x} \tag{9}$$

and decreases very rapidly as h increases outside this range. Then, as a first step towards a simple and reasonably accurate approximation we write (8) as

$$\sigma(x) = -\frac{\mu b}{2\pi(1-\nu)}\int_{-ar+x}^{ar+x} \frac{f(t)}{t-x}dt \tag{10}$$

where a is a constant of order unity. Expanding f(t) in a Taylor series about the point x this becomes

$$\sigma(x) = -\frac{\mu b}{2\pi(1-\nu)}\int_{-ar+x}^{ar+x} \frac{f(x)}{t-x} + \frac{df}{dx} + \frac{(t-x)}{2}\frac{d^2f}{dx^2} + \ldots dt \tag{11}$$

and we have

$$\sigma(x) = -\frac{\mu bar}{\pi(1-\nu)}\frac{df}{dx} \tag{12}$$

The latter approximation rests on the supposition that the contributions in (8) from terms involving higher derivatives of f(x) are small. As we shall see later, examination of the result

obtained in this way shows the error to be small except at points within ar of the ends of the cylinder. This approximation is justified by recognizing that we have neglected the terms

$$\frac{a^3r^3 + 3arx^2}{3}\frac{d^3f}{dx^3} + \ldots \tag{13}$$

This series for f(x) as defined in (11) is clearly convergent when x/l is small. The approximation adopted is acceptable provided the ratio of successive terms is sufficiently small. In particular, it is necessary that the ratio of the first neglected term is small compared with that retained. This ratio is

$$\frac{l^2}{3}\frac{a^2r^2 + x^2}{(l^2 - x^2)^2} \tag{14}$$

and is < 0.2 provided that $x < 0.75$. Similar conclusions follow for the ratios of further terms. Thus, the approximation is valid everywhere save at points close to the ends of the whiskers. From (5) and (7) we then have

$$\frac{\dot{\epsilon}x}{b} = -\frac{\mu b^2 Dar}{\pi(1-\nu)kT} f\frac{df}{dx} \tag{15}$$

whence

$$F = \left[\frac{\pi(1-\nu)}{\mu b^2}\frac{\dot{\epsilon}kT}{DAr}(l^2 - x^2)\right]^{1/2} \tag{16}$$

and

$$\sigma(x) \approx \left[\frac{\mu a\dot{\epsilon}kTr}{\pi(1-\nu)bD}\right]^{1/2}\frac{x}{(l^2 - x^2)^{1/2}} \tag{17}$$

$\sigma(x)$ is a shear stress which acts over the lateral surface of the cylinder and which produces a total force

$$2\pi r\int_0^l \sigma(x)dx \tag{18}$$

We equate this force to that derived from a uniform normal stress which acts parallel to the axis of the cylinder. This stress is given by

$$\frac{2}{r}\int_0^l \sigma(x)dx = [\frac{4\mu a\dot{\epsilon}kTl^2}{\pi(1-\nu)b^2Dr}]^{1/2} \quad (19)$$

Then on the basis that the aspect ratio (l/r) of the cylinders is large we suppose that the normal force in the cylinders associated with this stress must be balanced by one which operates in the matrix and which, to a first approximation is equivalent to a stress

$$\Delta\tau = \frac{2c}{1-c}[\frac{\mu a\dot{\epsilon}kTl^2}{\pi(1-\nu)b^2Dr}]^{1/2} \quad (20)$$

b. Comparison with experiment

To examine the effect of this stress on the observed strain rate we recognize that

$$\dot{\epsilon} = K\sigma^n \quad (21)$$

where σ is the operative stress. In the presence of fibers the operative stress becomes:

$$\tau - \Delta\tau = \tau - \alpha\dot{\epsilon} \quad (22)$$

On substitution of best estimates of the values appropriate for $MoSi_2$; μ = 100GPa; T = 1400K; l = 30μm; r =3μm; b= 0.3nm and with 20% of SiC we get, almost independent of ϵ, $\Delta\tau$ = 5MPa. This value, in view of the uncertainties in the values of the parameters, is in excellent agreement with that found at NRL by Sadananda[13], namely 10 MPa.

c. Implications

★ The analytic theory agrees with experiment.

d. Plans

★ Numerical computations will be performed to check the influence of the approximations in the analytic theory.

★ Comparison with experiment will be extended to a wider range of environments.

Task 120. Macroscopic stochastic model for creep

The methods of Boltzmann's classical statistical mechanics have been employed to calculate the yield strength in the absence of thermal activation in the case where hardening is due to randomly dispersed spherical particles.

a. Theory

We seek to determine the yield strength at 0K of a material hardened by the presence of spherical particles which act as simple blocks to the motion of dislocations. The analysis is based on a consideration of the stability of a sequence of lengths of a single dislocation which has impinged on spherical particles in the process of traversing a slip plane.

We assume that when acted on by a uniform stress σ, dislocations are bent into arcs of circles of radius R, where

$$\sigma = \frac{\mu b}{R} \tag{23}$$

μ is the shear modulus and b the magnitude of the Burgers vector; that impenetrable particles are randomly distributed and provide restraining forces of a magnitude which is related through an angle $\alpha(r)$ to the size r of the circle of intersection of particle and slip plane and which is specified by

$$F = \mu b^2 \sin \alpha(r) \tag{24}$$

and that the yield stress is the largest for which it is possible to have a stable dislocation join an infinite number of particles along a line which is essentially straight and hence does not cross itself.

Towards the determination of this stress we shall adapt the theoretical analysis given by Hanson and Morris[14] and by Labusch[15] for the yield strength due to such a dispersion of point obstacles all of which provide the same maximum restraining force of

$$F = \mu b^2 \sin\alpha \sim \alpha \mu b^2 \tag{25}$$

This analysis rests on the rolling circle technique employed by Foreman and Makin[16] in their numerical investigation of this hardening. Thus, it was argued (see Figure 5)

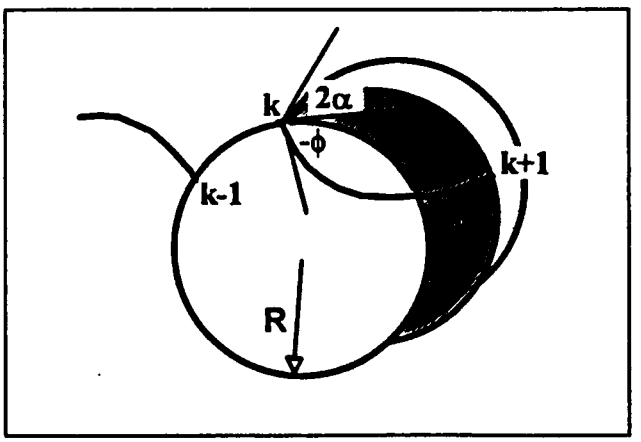

Figure 5 The rolling circle construction

that a dislocation stable at a sequence of positions ..., k-2, k-1 will also be stable at the next position k provided the particle associated with the k+1th position is centered anywhere in the region traversed by a rolling circle as shown hatched; this region is bounded by an angle $\theta \leq 2\alpha$. A particular characteristic of such sequences of dislocation lengths is that they must not cross themselves.

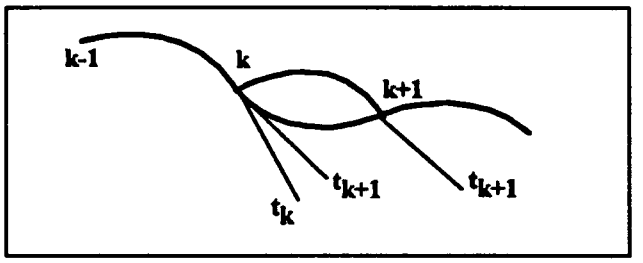

Figure 6 Relationship between t_k and t_{k+1}.

Here, we shall adapt the treatment of Hanson and Morris[14] to the case where the strength of a particular obstacle depends on the radius of the circle of intersection between the spherical particle concerned and the slip plane. To proceed, we note first from Figure 5, in the case of point obstacles that, following the path of a rolling circle, the angle turned between successive tangents, t_k, is equal to the angle ϕ which gives the direction of the trailing circle edge at the point of rotation (see Figure 6). It is then readily seen that in the case of an obstacle with radius r, the angle turned becomes

$$\bar{\phi} = \phi(1+\frac{r}{R}) = T\phi \tag{26}$$

Then, if the number of points is N and if the angle ϕ occurs n_i times we have

$$N = \sum_{i=1}^{n} n_i \tag{27}$$

and the total angle turned is

$$\Phi = \sum_{i=1}^{n} n_1\bar{\phi}_i \tag{28}$$

If N is indefinitely large but ϕ finite, the average value of ϕ_i is zero. In this case the whole dislocation line is either straight or contains equal numbers of complete clockwise and anticlockwise rotations. The latter configuration is a situation of low probability which we can neglect.

The procedure for the determination of the thermodynamic probability is akin to that employed to determine the Maxwell-Boltzmann distribution of kinetic energies in an ideal monatomic gas. Thus, if there are n partitions of i at each of N points the thermodynamic probability that the ith is employed n_i times is:

$$P = \frac{N! \prod_{i=1}^{n} p_i^{n_i}}{\prod_{i=1}^{n} n!} \tag{29}$$

where p_i is the occupational probability of the ith region. To determine p_i we divide the hatched area A into n regions of area δA_i (i = 1, n), each characterized by a value of ϕ, say ϕ_i and see that when the concentration is c the probability that a point k lies in a particular area δA_i is

$$p_i = 1 - \exp(-C\delta A_i) \approx C\delta A_i \tag{30}$$

provided the area δA_i is sufficiently small. On the basis that the most probable configuration of a system having a large number of parts is that which actually occurs, to determine this configuration we have only to maximize P subject to the constraints offered by (27) and (28). To proceed we take advantage of the facts that N and n_i are both large to employ Stirling's approximation and then

$$\delta \ln P = \sum_{i=1}^{n} \delta n_i + \ln p_i - \sum_{i=1}^{n} \ln n_i \tag{31}$$

while (27) and (28) become

$$\sum_{i=1}^{n} \delta n_i = 0 \tag{32}$$

$$\sum_{i=1}^{n} \delta n_i \bar{\phi}_i = 0 \tag{33}$$

Introducing the Lagrangian multipliers λ and γ we have

$$\ln p_i - \ln n_i + \gamma + \lambda \bar{\phi}_i = 0 \tag{34}$$

$$n_i = \frac{N p_i e^{\lambda_i}}{\sum_{i=1}^{n} p_i e^{\lambda \phi_i}} \tag{35}$$

then from (28) and (33) we have

$$N \sum_{i=1}^{n} e^{\lambda\Phi_i} \phi_i p_i = \Phi S \tag{36}$$

$$\sum_{i=1}^{n} \phi_i e^{\lambda\Phi_i} = S \tag{37}$$

and on substituting for n_i in the logarithm of P (31) we find, after some manipulation

$$P = S^N e^{-\lambda\Phi} \tag{38}$$

Then invoking (30) and (35) and proceeding to the limit of small quantities δA, (38) becomes

$$P = e^{-\lambda\Phi} [c\int e^{\lambda\bar{\Phi}} dA]^N \tag{39}$$

We have now to determine s and λ. Here, where A is the area indicated in fig. (1) we have

$$S = c\int_0^{2R} (l + r)dl \int_{T(\sin^{-1}(l/2R))}^{T(2\alpha - \sin^{-1}(l/2R))} e^{\lambda\Phi} d\Phi \tag{40}$$

The determination of λ is assisted by the realization that

$$\frac{d\ln S}{d\lambda} = \frac{1}{S}\frac{dS}{d\lambda} = \sum_{i=1}^{n} \frac{\phi_i e^{\lambda\phi_i} p_i}{S} = \frac{\Phi}{N} \to 0 \text{ as } N \to \infty \tag{41}$$

and λ must be such that

$$\frac{dS}{d\lambda} = 0 \tag{42}$$

This question can be resolved only by numerical means. In the special and unrealistic case in which $\alpha \ll 1$ we find, independent of the value of T, that $\lambda = 1.41/\alpha$.

b. Comparison with experiment

★ In comparison with the case treated previously[16] there are additional complications: the obstacles have finite radius and; because the radii of individual obstacles differ one from another, they have variable strengths. Bacon, Kocks and Scattergood[17] have shown through numerical studies that the Orowan stress, τ for a linear array of impenetrable circular blocks

to dislocation motion having radius R and inter-center spacing L is given by

$$\tau = \frac{\mu b}{4\pi} \frac{\ln X}{L - 2R} \tag{43}$$

where X is the harmonic mean of L and 2R (2). Thus, the specific strength of these obstacles is variable and denoted by the term $\ln X/2\pi$. Here, the obstacles are not distributed along a straight line nor regularly spaced. Additionally their strengths are variable. This additional work must be done before a comparison with experiment can be performed,

c. Implications

★ That the zero-temperature is analytically tractable means that we have a good measure against which to check more general numerical models.

d. Plans

★ The results will be used, for checking purposes, as the zero-temperature limit of the finite-temperature model planned in task 111.

Task 200. Lifetimes of piezoelectric ferroelectrics

The utility of PZT as a 'smart material' stems from its high dielectric constant, which gives large changes in polarization for quite small electric fields. Unfortunately, this property is linked to ferroelasticity, which can be destructive of the mechanical stability. It is this consequence, which leads to premature mechanical failure of sensors subjected to cyclic loading, which forms the critical issue.

a. Theory

In order to determine what can be done to address the critical issue, it is instructive to review the physics of ferroelectrics. The properties of PZT are primarily a consequence of a phase transition in which the crystal structure changes from cubic above the Curie temperature (about K) to body-centered tetragonal, with the c axis slightly longer than the a axes (0.5 to 3%, depending on composition). The cell-centering Zr/Ti atoms are positioned slightly off-center along the c-direction, so that each cell has a small, permanent electric dipole moment. In the as-transformed state the dipoles are arranged in small domains, with a volume fraction f = 1/3 oriented along each of the three crystal axes, so that there is no net polarization. The elastic energy is

$$U_{el} = \frac{1}{4}\mu(\delta\epsilon)^2 \ (1+3f)(1-f) \qquad (44)$$

where $\delta\epsilon$ is the transformation strain and f is the volume fraction of cells oriented with c-axis parallel to a particular crystal axis. It is clear that the elastic energy is a maximum for f=1/3. The electric energy (the interaction energy of the dipoles) will be a minimum for the same value of f. To produce a useful material, the material must be polarized, or 'poled'; that is, exposed for a short time (10-60 minutes) to a large electric field (of order 1-10 MV/m) at a temperature of about 450K, somewhat below the Curie temperature but above the service temperature. This causes a preferential orientation of the cell c-axes along the electric field axis, in a sense such that the dipoles lie as closely antiparallel as is possible to the applied field. This decreases the elastic energy, as can be seen from (44) if f is taken to be the volume fraction of dipoles lined up antiparallel to the field axis. The internal electric energy is increased, but the total electric energy decreases because of the negative energy of the antiparallel dipoles in the applied field. The material is then cooled and the electric field removed, leaving a low elastic energy, a high electric energy and a spontaneous polarization P_s. The poled state is never maximally polarized. The best that can be done is to rotate the dipoles within each grain to the crystal axis most closely parallel to the field direction, which may leave a dipole-field angle of up to 45°. Even this optimum polarization cannot be realized, because the dipole rotation causes grain boundary stresses to develop and increase to the point that further rotation is suppressed. Therefore the poled grains consist of domains which are differently oriented, but with a large net dipole moment in the direction of the applied field. That the unpoled and poled states are energetically metastable indicates that there is an energy barrier associated with the change; otherwise a transition to the ground state would occur spontaneously. Therefore changes in the polarization

take place by one or more thermally activated processes, for example domain nucleation and growth or domain wall motion. The magnitude of P_s after poling is of order 0.1 - 0.5 coulombs m^{-2}. The electrostatic energy density of a system of parallel dipoles in SI units is

$$U_{es} = \frac{p_0^2}{8\pi\kappa_0 v_a} \sum_i \frac{3\cos^2\theta_i - 1}{r_i^3} \tag{45}$$

where p_0 is the dipole size, κ_0 is the permittivity of free space, v_a is the volume of the unit cell. The sum is performed for a single dipole and is taken over all neighboring dipoles, with r_i the magnitude of the vector joining the origin to the ith neighbor and θ_i the angle between this vector and the dipole axis. For a cubic structure the sum in (45) vanishes by symmetry; therefore the magnitude of the electrostatic energy depends on the transformation strain $\delta\epsilon$ (in fact the dependence varies as $\delta\epsilon^2$, the same as the elastic energy). For $\delta\epsilon$ of 0.01, the sum in (45) has a value of about $0.1v_a$.

For a transformation strain of 0.01 and a shear modulus of 100GPa, the elastic energy of the unpoled state is about $3MJ/m^3$. In a completely poled state, with $P_s = 0.1 - 0.5C/m^2$, the electrostatic energy varies from 5 to $125MJ/m^3$. Although these are only approximate quantities, the indication is that the electrostatic energy stored during the poling process is substantially larger than the lost elastic energy. This means that the poled material exists in a relatively high-energy, metastable state.

Now attention will be turned to the question of premature failure under cyclic deformation, which occurs under conditions of mechanical loading[18] for quite moderate stress levels. The propensity toward mechanical instability is not surprising in view of the magnitude of the stored electrostatic energy, but the mechanism has yet to be determined. The specific experiments cited[18] involve cyclic bending such that the tensile and compressive stresses developed act normal to the poling axis. The larger part of the specimen, therefore, consists of domains in which the polarization, together with the c-axis, is oriented more normal than parallel to the stress. In the tensile part of the cycle, domain walls will migrate to favor domains oriented more parallel to the stress direction and new domains will nucleate and grow. This effect is analogous to the poling process in that the field-coupled elastic energy is increased, but is compensated by a negative work done by the applied stress. At the same time the electrostatic energy is reduced. When the tensile stress is released, the stored elastic energy becomes manifest as internal stresses, principally at the grain boundaries. Because the electrostatic energy in the poled state is so large, the elastic energy developed can be much larger than in the original, unpoled state and failure, most likely by intergranular fracture, is inevitable.

b. Comparison with experiment

The arguments above explain the basic physical reasons for failure, but not the specific mechanics. In the compressive cycle, the effects discussed above will be reversed, which negates

the simple rationalization. Therefore two observations remain to be explained.

1. According to the mechanism above, a simple monotonic tensile stress, applied for a sufficient time and then released, would be adequate for failure to occur by thermally activated creep of the domain structure. There are no explicit experimental measurements to confirm or refute this hypothesis. However, it is reasonable to expect that the effect would have been noticed and reported, if it occurred.

Domain walls are susceptible to pinning by defects[19]; these may be vacancies, substitutional inhomogeneities or, of course, grain boundaries. It is reasonable to expect that the response to a monotonic stress will be decay into a state in which all walls are pinned, so that further development of the substructure is inhibited. In fact the experimental results from NIST[18] show that the fracture stress at room temperature in monotonic bending is about 140MPa, or about 1.4 x $10^{-3}\mu$. This is a relatively low stress and may reflect a catastrophic release of energy which is likely to occur once a crack is nucleated.

2. Cyclic stressing, according to the same mechanism, should be completely reversible. However, experiment[18] shows that under cyclic stressing at 70% of the fracture stress, the lifetime is in excess of 10^7 cycles. At stress amplitudes from 75% to 95% of the fracture stress, the lifetime decreases sharply from 10^5 to 10^2 cycles (although the spread is large). Clearly, not only is there is a threshold stress, but there is also a cyclic irreversibility for stress levels in excess of the threshold.

The presence of a threshold stress is compatible with thermally activated domain wall motion. There are several reasons for irreversibility. The most obvious is that the processes of domain annihilation and nucleation are not reversible. Another stems from the pinning of domain walls, as discussed above. Once a wall segment is pinned, it cannot easily retrace its propagation path. Therefore wall motion in the depoling sense will not easily reverse, instead proceeding in the depoling sense by a ratchet mechanism. The depoling is associated with an increased elastic energy density, which will be manifest as steadily increasing internal stresses each time the applied cyclic stress is relaxed. A third reason for irreversibility results from the binding of dislocations to the domain walls. With a misfit of 1% at the interface between parallel and normal domains, a wall of length just a hundred lattice constants will accumulate a total misfit of a complete lattice constant; the energy of the wall can then be reduced substantially by forming a misfit dislocation, that is an edge dislocation with Burgers vector in the plane of the wall and with the extra half-plane lying always in the normal domain. Then wall motion is limited by the rate at which the dislocations can climb. In the tensile part of the cycle, the dislocations must climb by emitting interstitials (or absorbing vacancies), while in the compression phase, vacancies are emitted. Any asymmetry in these two processes will be manifest as an irreversibility. The advantage of this climb mechanism is that the predicted irreversibility is cumulative, a property not shared by the other irreversible processes discussed above. Finally, it is also important to look at the piezoelectric properties of PZT, even though the case in question involves mechanical loading at constant (=0) electric field. Consider the simple case in which the tensile/compressive stress σ_{11} lies along the x_1 axis and the poling axis

is x_3. Then there is a piezoelectric coupling

$$\Delta p_3 = d_{311}\sigma_{11} \tag{46}$$

where Δp_i is the polarization increment and d_{ijk} is the piezoelectric tensor. The coefficient d_{311} is negative, so that the dipoles lined up antiparallel to the poling axis are increased in magnitude. The dipoles normal to the poling axis, however, are unchanged. Therefore the electrostatic energy density becomes larger in the parallel (to the poling axis) domains than in the normal domains. This means that domain wall motion of such a sense as to increase the size of the normal domains (as is the case in tension) is accompanied by a small decrease in electrostatic energy and will be enhanced. In compression the energy in the parallel dipoles becomes smaller. Since the stress is reversed, the wall motion is reversed and is similarly enhanced. Thus the piezoelectric effect is completely reversible.

c. Implications

★ We conclude that the irreversibility which leads to failure of PZT in cyclic stressing is connected with ferroelastic domain wall motion and is not influenced by the piezoelectric character. If the problem is to be corrected, it is essential to determine the mechanism which controls domain wall mobility. To this purpose, both theory and experiment are required.

d. Plans

★ The mechanisms of ferroelastic domain wall motion will be modelled, with the aim of determining critical parameters which can be derived from or compared with experiment. Specific questions to be answered are:

1. Is the wall motion governed by the two-dimensional analog of kink pair nucleation and propagation, or by diffusive dragging of wall defects and dislocations?

2. How are these mechanisms influenced by an electric field of sufficient magnitude to stabilize the poled state?

3. How do the lifetimes of poled and unpoled specimens compare?

★ The theoretical work will be closely coordinated with experimental work at NIST and NRL.

References

1. M.S. Duesbery and K. Sadananda, Phil. Mag., 63 (1991) 535.
2. N.P. Louat, M.S. Duesbery, M.A. Imam, V. Provenzano and K. Sadananda, Phil. Mag. Lett., 63 (1991) 3.
3. M.S. Duesbery, N.P. Louat and K. Sadananda, unpublished work.
4. R. Ebeling and M.F. Ashby, Phil. Mag. 13 (1966) 805
5. S.D. Harkness and J.J. Hren, Met. Trans. 1 (1970) 43
6. D. Raynor and J.M. Silcock, Metal Science 4 (1970) 121
7. B. Noble, S.J. Harris and K. Dinsdale, Metal Science 16 (1982) 425
8. M.C. Chaturvedi and D.W. Chung, Met. Trans. A, 12A (1981) 77.
9. N. Hansen, Acta Met. 18 (1970) 137.
10. V.A. Phillips, Acta Met. 14 (1966) 1533.
11. F.J. Humphreys and J.W. Martin, Phil. Mag. 16 (1967) 927
12. F. Kroupa
13. K. Sadananda, private communication.
14. K. Hanson and J.W. Morris, Jr., J. Appl. Phys. 46 (1975) 983.
15. R. Labusch, J. Appl. Phys. 48 (1977) 4550.
16. A.E. Foreman and M.J. Makin, Phil. Mag. 14 (1966) 911.
17. D.J. Bacon, U.F. Kocks and R.O. Scattergood, Phil. Mag. 28 (1973) 1241.
18. G. White, NIST, private communication.
19. K. Yoo and S.B. Desu, Proc. Conf. on "Recent Advances in Adaptive and Sensory Materials and their Applications", Blacksburg VA, Technomic, Lancaster, 1992, p157.

Figure Captions

Figure 1 Definition of the geometric parameters D, L and θ.

Figure 2 An Orowan plot of strength for dispersion hardened materials.

Figure 3 Plot of strength following the unified approach of equation (2).

Figure 4 The distribution of breaking angles.

Figure 5 The rolling circle construction.

Figure 6 Relationship between t_k and t_{k+1}.

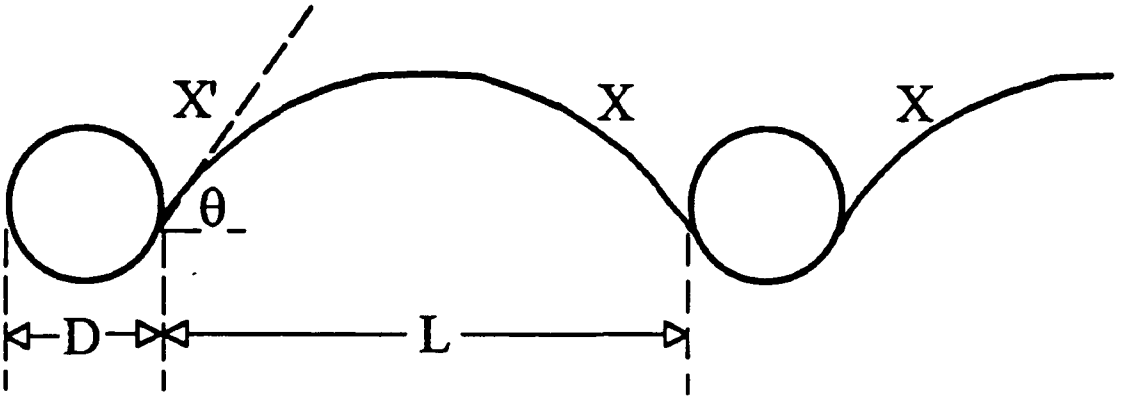

FIG. 1

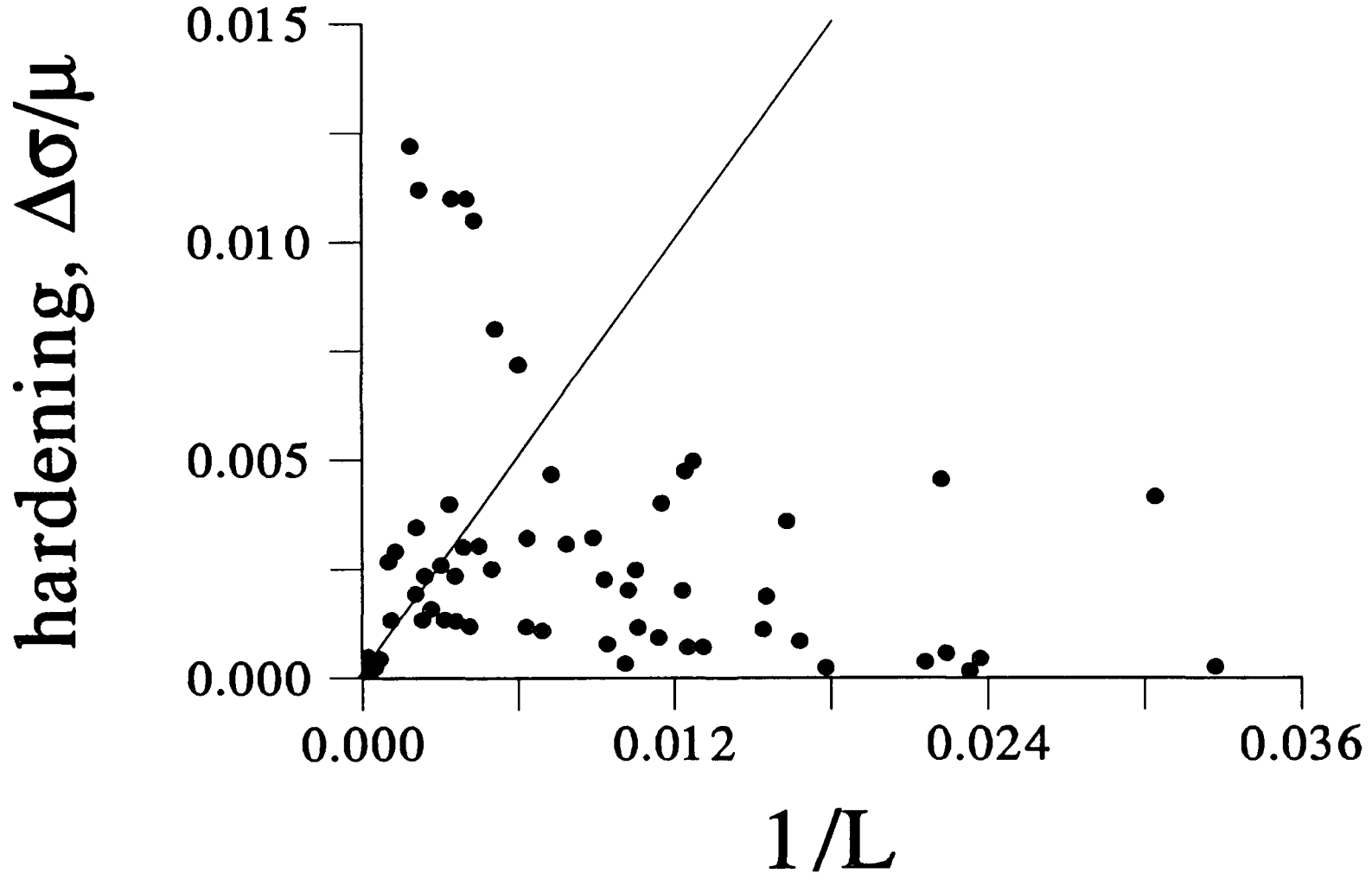

FIG. 2

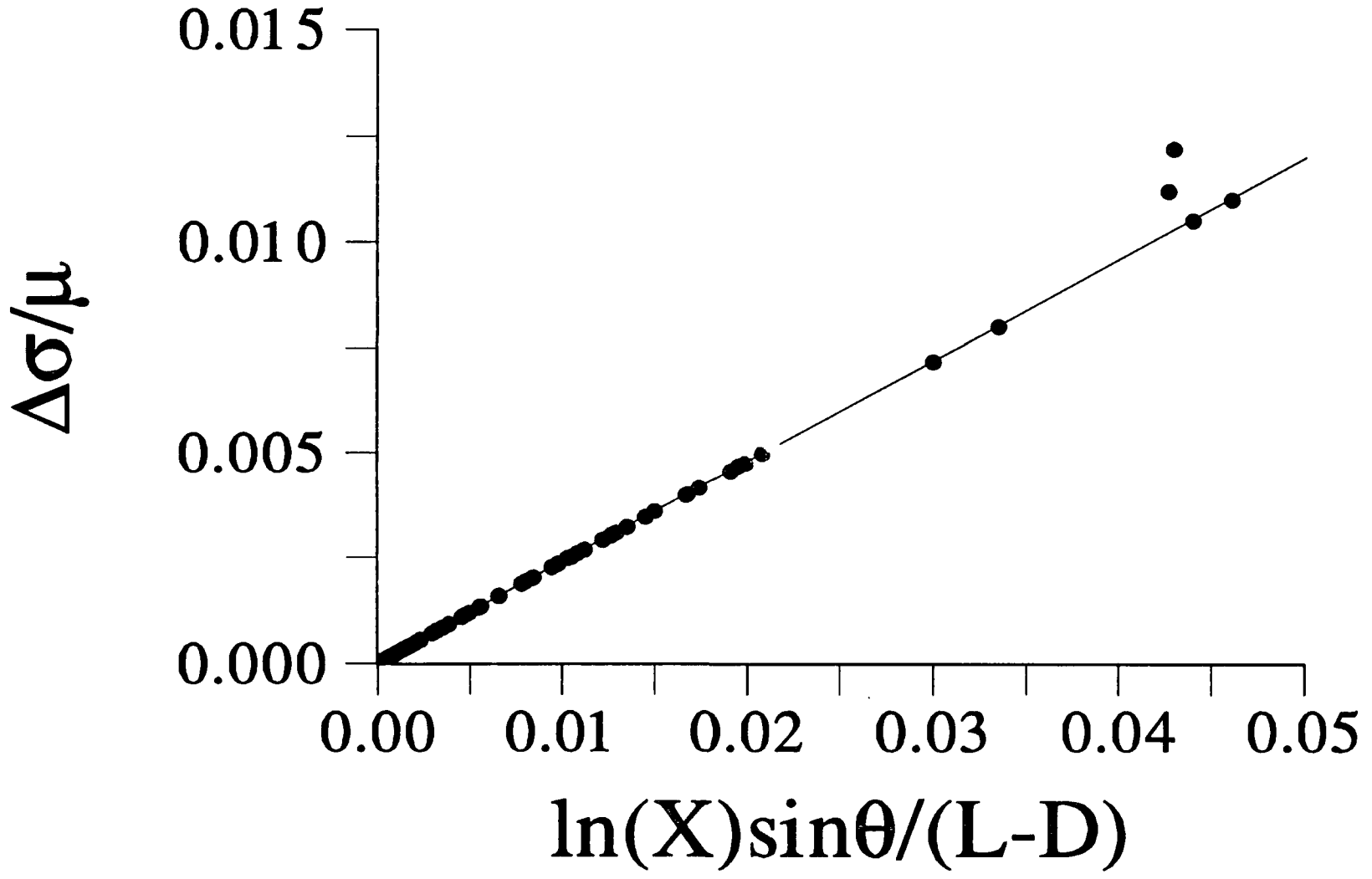

FIG. 3

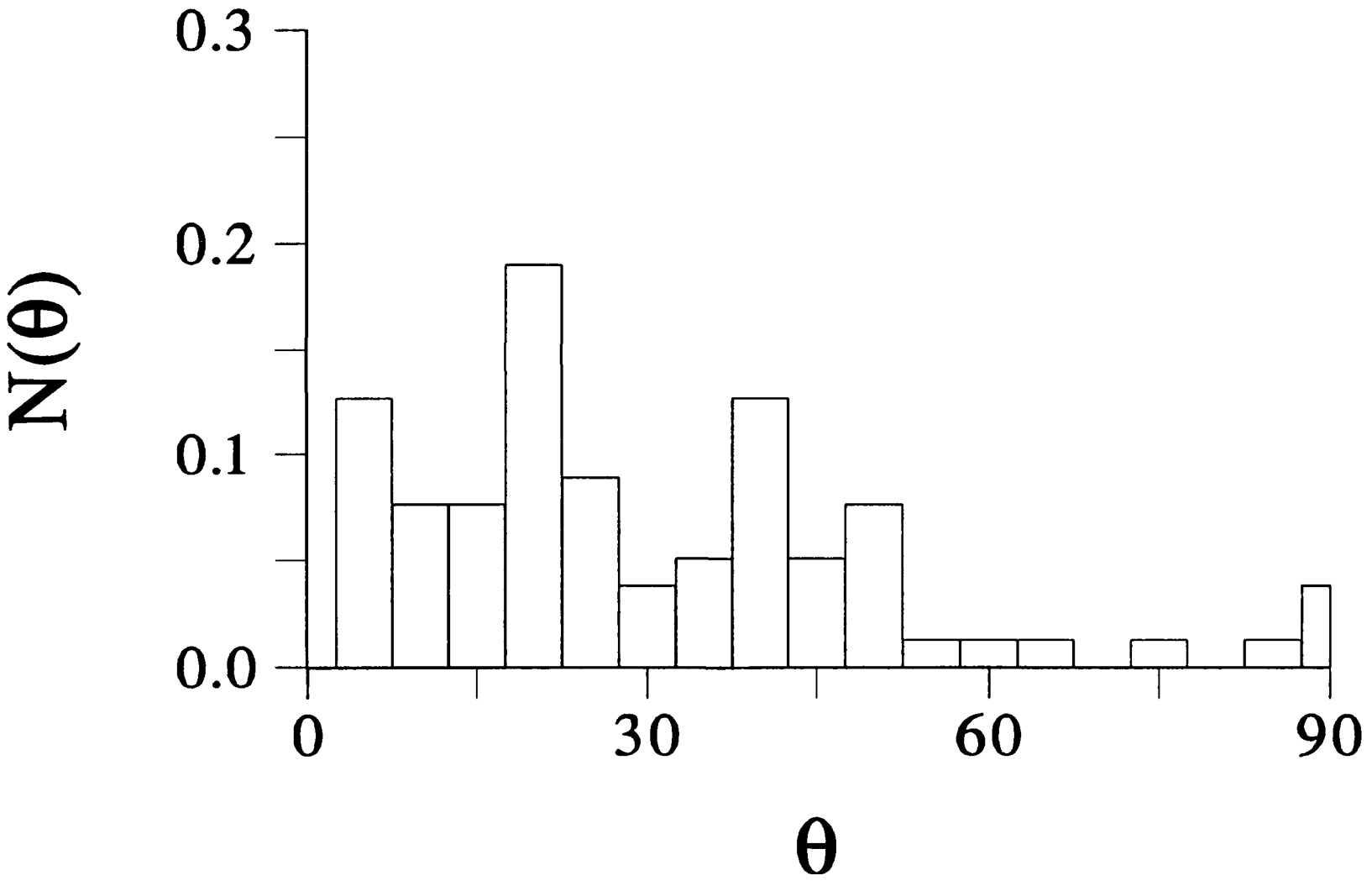

FIG. 4

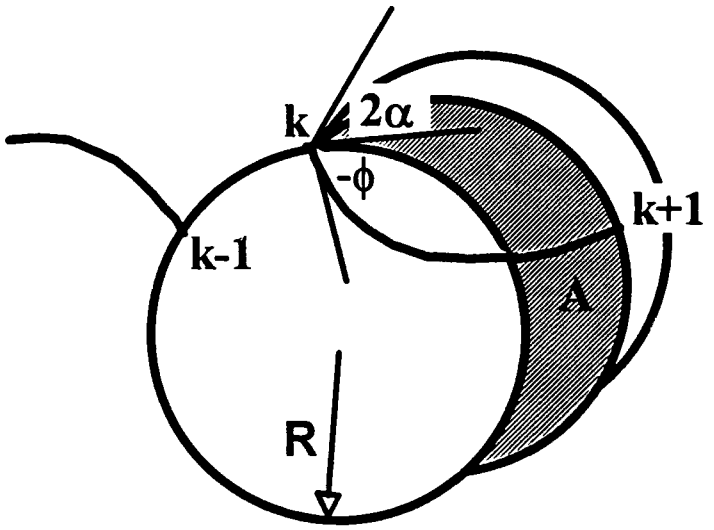

FIG. 5

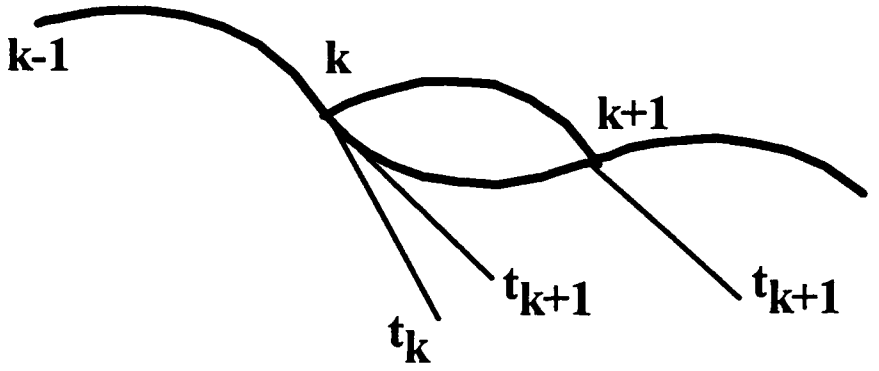

FIG. 6